RSC Advances

PAPER

View Article Online
View Journal | View Issue

Cite this: *RSC Adv.*, 2024, **14**, 6521

Symmetric dicyanobenzothiadiazole (DCBT) dyes with a 1.5 eV excited state reduction potential range†

Qing Yun Li, [a] Ethan C. Lambert, [a] Ravinder Kaur, [a] Nathan I. Hammer [a] and Jared H. Delcamp *[ab]

Received 27th September 2023
Accepted 23rd January 2024

DOI: 10.1039/d3ra06575h

rsc.li/rsc-advances

Strong molecular photooxidants are important in many disciplines including organic synthesis and renewable energy. In these fields, strongly oxidizing chromophores are employed to drive various transformations from challenging bond formations to energy storage systems. A range of photooxidant strengths are needed to drive these processes. A series of 8 symmetrically bisarylated 5,6-dicyano[2,1,3]benzothiadiazole (DCBT) dyes were studied for their tunability toward breadth of light absorption and photooxidant strength. The dye oxidation strength and light absorption tunability is the result of appending various aryl substituents on the periphery of the DCBT core which shows remarkable tunability of the final chromophore. The dyes are studied *via* steady-state absorption and emission, time-correlated single photon counting, computational analysis, and cyclic voltammetry. In changing the peripheral aryl substituents *via* electronics, sterics, and π-conjugation length, a series of dyes are arrived at with a dramatic 1.5 eV range in oxidizing strength and >200 nm (0.95 eV) absorption maxima tunability. Furthermore, two dyes in the series exhibit strong oxidizing strength while still approaching red light absorbance (>650 nm onset) which provides unique opportunities for the use of lower energy light to affect chemical transformations. Ultimately, this series provides options for photooxidations that allow for energetic tuning and selectivity for a given chemical transformation.

Introduction

Strong photooxidants are of interest in multiple fields such as sustainable synthetic chemistry[1–9] and solar-to-fuel generation.[10–18] In these systems, a strong photooxidant is often used to create greater driving forces in order to achieve higher efficiencies and to access new reactions.[4,19–23] Depending on the photooxidant used, selectivity towards certain processes can also be increased.[23–26] Molecular photooxidants are often characterized by two important features, oxidizing strength as well as excited state (ES) lifetime. Thus, literature known photooxidants are commonly metal-based, such as $[Ru(bpy)_3]^{2+}$, given that organic photosensitizers often have short-lived excited state lifetimes in the nanosecond regime.[27] However, organic dyes exhibiting much longer ES lifetimes in the microsecond regime are becoming more common such as with the widely studied acridinium based photooxidants.[8,19,23] More recently, a series of benzo[*c*][1,2,5]thiadiazole-5,6-dicarbonitrile (DCBT) based dyes have been synthesized and studied for their photooxidizing abilities to reveal a dye (QL11) of strong oxidizing strength as well as a long lived ES lifetime (16 μs measured by transient absorption spectroscopy).[28]

The exceptionally withdrawn nature of the DCBT core makes it an ideal addition to a strong photooxidant systems since this core can be used in photoinduced charge transfer systems to oxidize weakly donating groups appended to it.[29] While the literature known DCBT dyes showcased symmetric and asymmetric moieties, the symmetric photosensitizers exhibited greater oxidizing strength as well as longer lived excited state lifetimes in comparison to their asymmetric counterparts,[28] making symmetric DCBT dyes of greater interest and the focus of this work. Furthermore, the ease of synthetic access to a symmetric, doubly aryl substituted derivative allows for rapidly accessed dyes, resulting in an array of photooxidants of varying oxidation strengths.[28,29]

In this report, a series of six new symmetrical DCBT based dyes were synthesized along with 3 known dyes (Fig. 1). All 9 dyes were studied in order to assess the effect of the varying aryl groups on the oxidizing ability of the molecule. As previously shown, the energetics of a DCBT dye is highly tunable through the usage of various aryl substituents.[28] A range of electronic effects are probed through derivatives containing a cyano

[a]*Department of Chemistry and Biochemistry, University of Mississippi, University, 322 Coulter Hall, MS 38677, USA. E-mail: delcamp@olemiss.edu*

[b]*Materials and Manufacturing Directorate, Air Force Research Laboratory, 2230 Tenth Street, Wright-Patterson AFB, OH 45433, USA*

† Electronic supplementary information (ESI) available: Computational data, spectroscopic and electrochemical data, and NMR spectra. See DOI: https://doi.org/10.1039/d3ra06575h

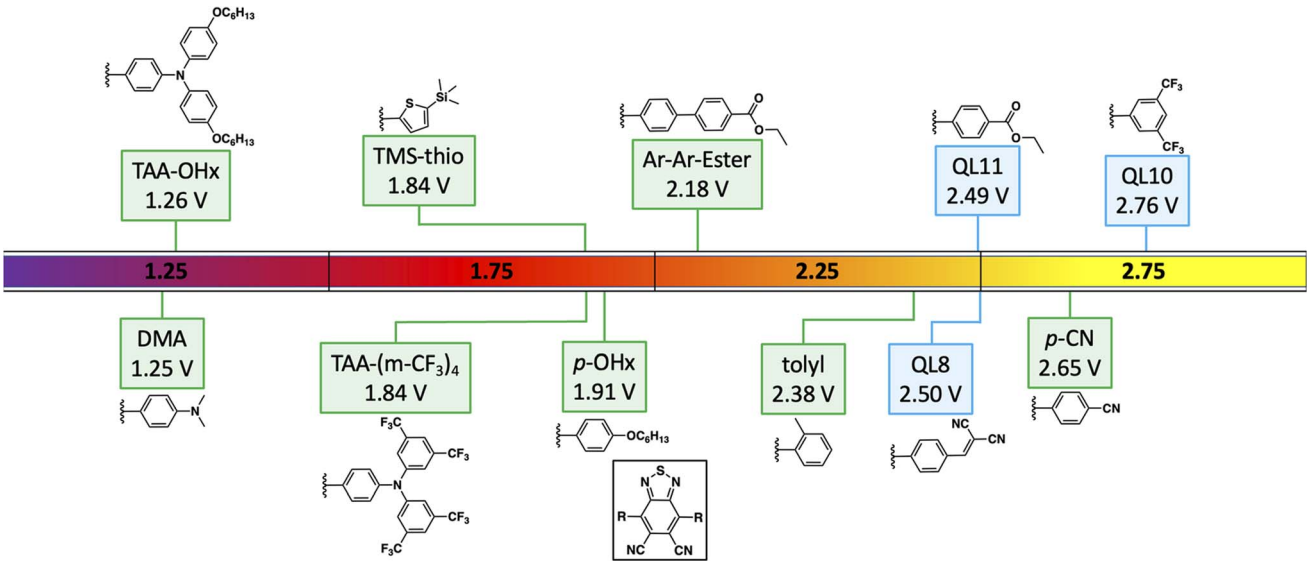

Fig. 1 Previously reported (aryl)$_2$DCBT dyes[28,29] (with QL codes) and the new dyes presented in this work. Potential values are *versus* normal hydrogen electrode (NHE).

group, an alkoxy group, thiophene, and multiple amine groups with varying donation strength. A tolyl derivative is also synthesized to test the effect of increased steric hindrance inducing a twisted π-system. Furthermore, a derivative featuring an extra phenyl spacer is also synthesized to see the effects of extended π-conjugation.

Experimental section

General information

All commercially obtained reagents were used as received. Benzo[*c*][1,2,5]thiadiazole-5,6-dicarbonitrile (**1**), 4-bromo-*N*,*N*-bis(4-(hexyloxy)phenyl)aniline (**TAA-(OHx)-Br**), and (5-bromothiophen-2-yl)trimethylsilane (**TMS-thio-Br**) show in Scheme 1 were prepared following literature precedent.[30–32] Thin-layer chromatography (TLC) was conducted with Sorbtech silica XHL TLC plates and visualized with UV light. Flash column chromatography was performed with Sorbent Tech P60, 40–63 μm (230–400 mesh). Flash column chromatography was performed using a Teledyne CombiFlash Rf + system. The silica gel cartridges were purchased from Luknova SuperSep (FC003012, 50 μm). ^{1}H and ^{13}C{^{1}H} NMR spectra were recorded on either a Bruker Avance-400 (400 MHz) or Bruker Avance-300 (300 MHz) instrument and are reported in ppm using solvent as an internal standard ($CDCl_3$ at 7.26 ppm, $(CD_3)_2CO$ at 2.05 ppm). Data reported as s = singlet, d = doublet, t = triplet, q = quartet, p = pentet, m = multiplet, br = broad, ap = apparent, dd = doublet of doublets; coupling constant(s) in Hz. UV spectra were measured with a Cary 5000 UV-Vis-NIR spectrometer. Emission spectra were measured with a Horiba FluoroMax SpectroFluorimeter. Curves were fitted with the LOESS function in Igor which allows for easier data interpretation and comparisons. Molar absorptivities were measured with an AvaSpec-ULS2048-USB2-50 Spectrometer (Pine Research part RRAVSP3), and the light source was a UV/Vis/NIR

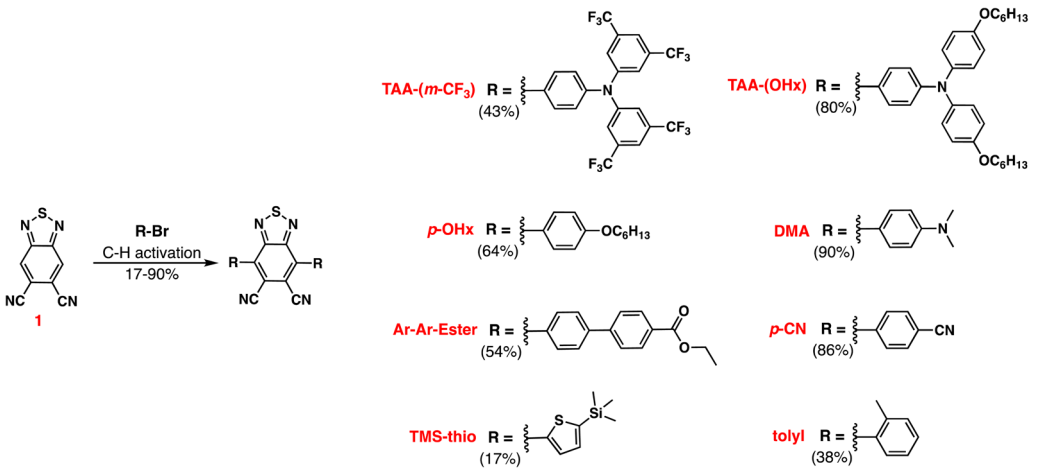

Scheme 1 Synthetic route to the DCBT dyes.

Light Source (Pine Research part RRAVSP). These two systems were used in conjunction with the AvaSoft8 software program. Cyclic voltammetry curves were measured with a C–H Instruments electrochemical analyzer CHI600E. Tetrabutylammonium hexafluorophosphate (0.1 M in dichloromethane) was used as the electrolyte. The working electrode is glassy carbon, the pseudo-reference electrode is a silver wire, and the counter electrode is platinum. A scan rate of 100 mV s^{-1} was used. Ferrocenium/ferrocene is used as an internal standard (taken as 0.70 V *vs.* normal hydrogen electrode (NHE) in dichloromethane (DCM)).[33,34] For electrospray ionization (ESI) high resolution mass spectrometry (HRMS), a quadruple-TOF system was used to obtain the data both in positive and negative modes with a Waters Synapt HDMS. IR experiments were recorded on a Bruker Alpha FT-IR spectrometer.

Computational approach

Molecules were drawn in ChemDraw (19.1.0.5) and saved as an MDL Molfile. Molecular geometries of the considered species were then optimized with the MMFF94 force field *via* Avogadro (1.2.0). Dihedral angles about non-cyclic single bonds were set to between 0 and 90 degrees manually to avoid local minima conformations. Accurate geometry optimization were performed sequentially by DFT using Gaussian 16 (ref. 35) with the M06-2X[36] functional applying the following basis sets: first 3–21g, second 6-31G(d,p),[37] and finally 6-311G(d,p).[37] Time dependent-DFT (TD-DFT) computations were performed with optimized geometries with the M06-2X functional and 6-311G(d,p) basis set to compute the vertical transition energies and oscillator strengths. This functional and basis set were previously found to have good agreement with experimental findings for DCBT dyes.[28]

Time-correlated single photon counting (TCSPC)

Emission lifetime curves were obtained using the 375 nm, 405 nm, or 485 nm line of an LDH series 405B pulsed diode laser (pulse width approx. 100 ps) as the excitation source and emission was detected using a PicoQuant PDM series single photon avalanche diode (time resolution approx. 50 ps) and a TimeHarp 260 time-correlated single photon counter (25 ps resolution). Appropriate filters were placed before the sample and detector. Time-resolved emission kinetics were best modeled by a single exponential function. Fluorescene lifetime values were measured in dichloromethane (5×10^{-4} M).

Synthetic protocols

***N*-(3,5-Bis(trifluoromethyl)phenyl)-*N*-(4-bromophenyl)-3,5-bis(trifluoromethyl)aniline (TAA-(*m*-CF_3)$_4$-Br).** Into a flame dried flask equipped with a stir bar and flushed with nitrogen, 4-bromoaniline (1.00 g, 5.81 mmol), 1-iodo-3,5-bis(trifluoromethyl)benzene (2.57 mL, 14.54 mmol), CuI (0.11 g, 0.58 mmol), 1,10-phenanthroline (0.21 g, 1.16 mmol), and KOH (5.30 g, 93.02 mmol) were dissolved in dry toluene (11.6 mL). The reaction was heated to reflux and monitored for completion by observing the disappearance of starting material *via* NMR. Once the reaction was complete, the mixture was then extracted with dichloromethane and water. The organic layer was then filtered through a thin pad of silica with 100% diethyl ether as the eluent and then concentrated under reduced pressure. The crude material was purified *via* silica gel chromatography with 20% dichloromethane/80% hexanes to yield a mostly pure mixture. This mixture is then washed with minimal hexanes 3 times, collecting the insoluble solid as the product each time to yield the pure product (**TAA-(*m*-CF_3)$_4$-Br**) (2.05 g, 59%). ^{1}H NMR (400 MHz, $CDCl_3$) δ 7.60–7.50 (m, 4H), 7.44 (s, 4H), 7.02 (d, J = 8.7 Hz, 2H) ppm. ^{13}C {^{1}H} NMR (100 MHz, $CDCl_3$) δ 147.7, 144.0, 134.0, 133.6 (J = 33.5 Hz), 127.4, 122.9, 122.9 (J = 271 Hz), 119.9, 117.4 ppm. ^{19}F NMR (376 MHz, $CDCl_3$) δ −63.1 ppm. IR (neat, cm^{-1}): 3101, 3072, 1469, 1377, 1276, 1121, 1007, 882, 835, 714, 701, 682, 656, 505. HRMS ESI (negative mode) m/z calc'd for $C_{22}H_9BrF_{12}N$ $[M - H]^-$ 593.9727, found 593.9756.

Ethyl 4′-bromo-[1,1′-biphenyl]-4-carboxylate (Ar-Ar-Ester-Br). Into a flame dried flask equipped with a stir bar and flushed with nitrogen, (4-(ethoxycarbonyl)phenyl)boronic acid (0.50 g, 2.58 mmol), 1,4-dibromobenzene (3.04 g, 12.89 mmol), K_3PO_4 (1.64 g, 7.73 mmol), and water (2.1 mL) were dissolved in dry toluene (52 mL). The mixture is degassed with nitrogen for 10 minutes. Pd_2dba_3 (236 mg, 0.26 mmol) and XPhos (246 mg, 0.58 mmol) were then added, and the mixture is heated to 90 °C. The reaction is monitored *via* NMR for the disappearance of the boron starting material. Once the reaction was complete, the mixture was then extracted with diethyl ether and water. The organic layer was dried with sodium sulfate and concentrated under reduced pressure. The crude material was purified *via* silica gel column chromatography with 25% dichloromethane/75% hexanes as the eluent to yield the pure product (**Ar-Ar-Ester-Br**) (275 mg, 35%). This compound has been previously synthesized and characterized; thus ^{1}H NMR shifts of the product were compared and found to be consistent with literature reported data.[38] ^{1}H NMR (300 MHz, $CDCl_3$) δ 8.11 (d, J = 8.5 Hz, 2H), 7.64–7.56 (m, 4H), 7.49 (d, J = 8.6 Hz, 2H), 4.41 (q, J = 7.1 Hz, 2H), 1.42 (t, J = 7.1 Hz, 3H) ppm.

4,7-Bis(4-(bis(3,5-bis(trifluoromethyl)phenyl)amino)phenyl) benzo[*c*][1,2,5]thiadiazole-5,6-dicarbonitrile ((TAA-(*m*-CF_3)$_4$)$_2$-DCBT). Into a flame-dried pressure flask flushed with Ar was added benzo[*c*][1,2,5]thiadiazole-5,6-dicarbonitrile (**1**) (50 mg, 0.27 mmol), *N*-(3,5-bis(trifluoromethyl)phenyl)-*N*-(4-bromophenyl)-3,5-bis(trifluoromethyl)aniline (**TAA-(*m*-CF_3)$_4$-Br**) (352 mg, 0.59 mmol), pivalic acid (27 mg, 0.27 mmol), K_2CO_3 (111 mg, 0.81 mmol), Pd_2dba_3 (25 mg, 0.027 mmol), and $[BF_4][HP(t\text{-}Bu)_2Me]$ (13 mg, 0.054 mmol) dissolved in dry toluene (0.9 mL). The flask was sealed and heated to 110 °C with monitoring of the reaction by NMR until complete consumption of the benzothiadiazole starting material (**1**). The mixture was then extracted with dichloromethane and water. The organics were dried with sodium sulfate and concentrated under reduced pressure. The crude product was purified *via* silica gel chromatography with 50% dichloromethane/50% hexanes as the eluent to yield pure product (**(TAA-(*m*-CF_3)$_4$)$_2$DCBT**) (141 mg, 43%). ^{1}H NMR (400 MHz, $CDCl_3$) δ 7.90 (d, J = 8.4 Hz, 4H), 7.67 (s, 4H), 7.61 (s, 8H), 7.32 (d, J = 8.4 Hz, 4H) ppm. ^{13}C {^{1}H} NMR (100 MHz, $CDCl_3$) δ 154.3, 147.5, 147.5, 140.3, 133.9 (J = 33.6 Hz), 132.8, 129.3, 124.3, 124.0, 122.9 (J = 267.9 Hz), 118.4, 115.5,

112.7 ppm. ^{19}F NMR (376 MHz, $CDCl_3$) δ −63.1 ppm. IR (neat, cm^{-1}): 2960, 2923, 2851, 1374, 1276, 1121, 1006, 884, 702, 682, 529, 403. HRMS ESI (positive mode) *m*/*z* calc'd for $C_{52}H_{21}F_{24}N_6S$ $[M + H]^+$ 1217.1165, found 1217.1173.

4,7-Bis(4-(hexyloxy)phenyl)benzo[*c*][1,2,5]thiadiazole-5,6-dicarbonitrile ((*p*-OHx)$_2$DCBT). Into a flame-dried pressure flask flushed with Ar was added benzo[*c*][1,2,5]thiadiazole-5,6-dicarbonitrile (**1**) (75 mg, 0.40 mmol), 1-bromo-4-(hexyloxy) benzene (***p*-OHx-Br**) (228 mg, 0.89 mmol), pivalic acid (41 mg, 0.40 mmol), K_2CO_3 (167 mg, 1.21 mmol), $Pd(OAc)_2$ (5 mg, 0.020 mmol), and $[BF_4][HP(t\text{-}Bu)_2Me]$ (10 mg, 0.040 mmol) dissolved in dry toluene (1.3 mL). The flask was sealed and heated to 120 °C with monitoring of the reaction by NMR until complete consumption of the benzothiadiazole starting material (**1**). The mixture was then extracted with dichloromethane and water. The organics were dried with sodium sulfate and concentrated under reduced pressure. The crude product was purified *via* silica gel chromatography with 80% dichloromethane/20% hexanes as the eluent to yield pure product (**(*p*-OHx)$_2$DCBT**) (139 mg, 64%). ^{1}H NMR (400 MHz, $CDCl_3$) δ 7.77 (d, J = 8.7 Hz, 4H), 7.12 (d, J = 8.8 Hz, 4H), 4.07 (t, J = 6.5 Hz, 4H), 1.84 (*p*, J = 6.7 Hz, 4H), 1.53–1.44 (m, 4H), 1.44–1.30 (m, 8H), 0.93 (t, J = 6.7 Hz, 6H) ppm. ^{13}C {^{1}H} NMR (100 MHz, $CDCl_3$) δ 161.3, 154.6, 141.0, 131.9, 124.6, 115.9, 114.9, 112.0, 68.3, 31.6, 29.2, 25.7, 22.6, 14.1 ppm. IR (neat, cm^{-1}): 2954, 2931, 2861, 2224, 1603, 1513, 1452, 1246, 1181, 1032, 837, 552. HRMS ESI (positive mode) *m*/*z* calc'd for $C_{32}H_{35}N_4O_2S$ $[M + H]^+$ 539.2481, found 539.2450.

Diethyl 4′,4‴-(5,6-dicyanobenzo[*c*][1,2,5]thiadiazole-4,7-diyl) bis([1,1′-biphenyl]-4-carboxylate) ((Ar-Ar-Ester)$_2$DCBT). Into a flame-dried pressure flask flushed with N_2 was added benzo[*c*][1,2,5]thiadiazole-5,6-dicarbonitrile (**1**) (50 mg, 0.27 mmol), ethyl 4′-bromo-[1,1′-biphenyl]-4-carboxylate (**Ar-Ar-Ester-Br**) (180 mg, 0.59 mmol), pivalic acid (27 mg, 0.27 mmol), K_2CO_3 (111 mg, 0.81 mmol), $Pd(OAc)_2$ (3 mg, 0.013 mmol), and $[BF_4][HP(t\text{-}Bu)_2Me]$ (7 mg, 0.027 mmol) dissolved in dry toluene (0.9 mL). The flask was sealed and heated to 120 °C with monitoring of the reaction by NMR until complete consumption of the benzothiadiazole starting material (**1**). The mixture was then extracted with dichloromethane and water. The organics were dried with sodium sulfate and concentrated under reduced pressure. The crude product was purified *via* silica gel chromatography with 55% acetone/45% hexanes as the eluent to yield pure product (**(Ar-Ar-Ester)$_2$DCBT**) (92 mg, 54%). ^{1}H NMR (400 MHz, $CDCl_3$) δ 8.19 (d, J = 8.4 Hz, 4H), 7.95 (d, J = 8.4 Hz, 4H), 7.90 (d, J = 8.4 Hz, 4H), 7.78 (d, J = 8.4 Hz, 4H), 4.43 (q, J = 7.1 Hz, 4H), 1.44 (t, J = 7.1 Hz, 6H) ppm. ^{13}C {^{1}H} NMR (100 MHz, $CDCl_3$) δ 166.5, 154.4, 144.3, 142.7, 141.4, 132.3, 131.1, 130.4, 130.2, 128.0, 127.4, 115.5, 112.9, 61.3, 14.5 ppm. IR (neat, cm^{-1}): 2974, 2927, 2903, 2228, 1700, 1604, 1454, 1364, 1271, 1178, 1102, 1003, 823, 772, 738, 701, 550. HRMS ESI (positive mode) *m*/*z* calc'd for $C_{38}H_{27}N_4O_4S$ $[M + H]^+$ 635.1753, found 635.1725.

4,7-Bis(5-(trimethylsilyl)thiophen-2-yl)benzo[*c*][1,2,5] thiadiazole-5,6-dicarbonitrile ((TMS-thio)$_2$DCBT). Into a flame-dried pressure flask flushed with N_2 was added benzo[*c*][1,2,5] thiadiazole-5,6-dicarbonitrile (**1**) (50 mg, 0.27 mmol), (5-bromothiophen-2-yl)trimethylsilane (**TMS-thio-Br**) (139 mg, 0.59 mmol), pivalic acid (27 mg, 0.27 mmol), K_2CO_3 (111 mg, 0.81 mmol), Pd_2dba_3 (25 mg, 0.027), and $[BF_4][HP(t\text{-}Bu)_2Me]$ (13 mg, 0.054 mmol) were dissolved in toluene (0.9 mL). The flask was sealed and heated to 110 °C with monitoring of the reaction by NMR until complete consumption of the benzothiadiazole starting material (**1**). The mixture was then extracted with dichloromethane and water. The organics were dried with sodium sulfate and concentrated under reduced pressure. The crude product was purified *via* silica gel chromatography with 40% dichloromethane/60% hexanes as the eluent to yield pure product (**(TMS-thio)$_2$DCBT**) (23 mg, 17%). This compound has been previously synthesized and characterized; thus ^{1}H NMR shifts of the product were compared and found to be consistent with literature reported data.[29] ^{1}H NMR (400 MHz, $CDCl_3$) δ 8.20 (d, J = 3.7 Hz, 2H), 7.41 (d, J = 3.7 Hz, 2H), 0.42 (s, 18H) ppm.

4,7-Bis(4-(bis(4-(hexyloxy)phenyl)amino)phenyl)benzo[*c*] [1,2,5]thiadiazole-5,6-dicarbonitrile ((TAA-(OHx))$_2$DCBT). Into a flame-dried pressure flask flushed with Ar was added benzo[*c*] [1,2,5]thiadiazole-5,6-dicarbonitrile (**1**) (50 mg, 0.27 mmol), 4-bromo-*N*,*N*-bis(4-(hexyloxy)phenyl)aniline (**TAA-(OHx)-Br**) (310 mg, 0.59 mmol), pivalic acid (27 mg, 0.27 mmol), K_2CO_3 (111 mg, 0.81 mmol), Pd_2dba_3 (25 mg, 0.027), and $[BF_4][HP(t\text{-}Bu)_2Me]$ (13 mg, 0.054 mmol) were dissolved in toluene (0.9 mL). The flask was sealed and heated to 110 °C with monitoring of the reaction by NMR until complete consumption of the benzothiadiazole starting material (**1**). The mixture was then extracted with dichloromethane and water. The organics were dried with sodium sulfate and concentrated under reduced pressure. The crude product was purified *via* silica gel chromatography with 50% dichloromethane/50% hexanes as the eluent to yield pure product (**(TAA-(OHx))$_2$DCBT**) (231 mg, 80%). ^{1}H NMR (300 MHz, $(CD_3)_2CO$) δ 7.71 (d, J = 8.9 Hz, 4H), 7.22 (d, J = 8.9 Hz, 8H), 7.03–6.91 (m, 12H) 4.02 (t, J = 6.5 Hz, 8H), 1.78 (*p*, 8H), 1.55–1.30 (m, 24H), 0.91 (t, J = 7.0 Hz, 12H) ppm. ^{13}C {^{1}H} NMR (75 MHz, $(CD_3)_2CO$) δ 157.9, 155.7, 152.0, 141.4, 140.4, 132.7, 129.1, 124.5, 117.8, 117.4, 116.6, 112.0, 69.0, 32.5, 30.2, 26.6, 23.4, 14.5 ppm. IR (neat, cm^{-1}): 3040, 2925, 2856, 2224, 1596, 1502, 1448, 1323, 1235, 1194, 1160, 826. HRMS ESI (positive mode) *m*/*z* calc'd for $C_{68}H_{77}N_6O_4S$ $[M + H]^+$ 1073.5727, found 1073.5721.

4,7-Bis(4-(dimethylamino)phenyl)benzo[*c*][1,2,5]thiadiazole-5,6-dicarbonitrile ((DMA)$_2$DCBT). Into a flame-dried pressure flask flushed with Ar was added benzo[*c*][1,2,5]thiadiazole-5,6-dicarbonitrile (**1**) (50 mg, 0.27 mmol), 4-bromo-*N*,*N*-dimethylaniline (**DMA-Br**) (118 mg, 0.59 mmol), pivalic acid (27 mg, 0.27 mmol), K_2CO_3 (111 mg, 0.81 mmol), Pd_2dba_3 (25 mg, 0.027), and $[BF_4][HP(t\text{-}Bu)_2Me]$ (13 mg, 0.054 mmol) were dissolved in toluene (0.9 mL). The flask was sealed and heated to 110 °C with monitoring of the reaction by NMR until complete consumption of the benzothiadiazole starting material (**1**). The mixture was then extracted with dichloromethane and water. The organics were dried with sodium sulfate and concentrated under reduced pressure. The crude product was purified *via* silica gel chromatography with 40% ethyl acetate/60% hexanes as the eluent to yield pure product (**(DMA)$_2$DCBT**) (103 mg, 90%). This compound has been previously synthesized and

characterized; thus ^{1}H NMR shifts of the product were compared and found to be consistent with literature reported data.[29] ^{1}H NMR (400 MHz, $CDCl_3$) δ 7.77 (d, $J = 9.0$ Hz, 4H), 6.87 (d, $J = 8.9$ Hz, 4H), 3.09 (s, 12H) ppm.

4,7-Bis(4-cyanophenyl)benzo[*c*][1,2,5]thiadiazole-5,6-dicarbonitrile ((*p*-CN)$_2$DCBT). Into a flame-dried pressure flask flushed with N_2 was added benzo[*c*][1,2,5]thiadiazole-5,6-dicarbonitrile (**1**) (50 mg, 0.27 mmol), 4-bromobenzonitrile (***p*-CN-Br**) (108 mg, 0.59 mmol), pivalic acid (27 mg, 0.27 mmol), K_2CO_3 (111 mg, 0.81 mmol), $Pd(OAc)_2$ (3 mg, 0.013 mmol), and $[BF_4][HP(t\text{-}Bu)_2Me]$ (7 mg, 0.027 mmol) dissolved in dry toluene (0.9 mL). The flask was sealed and heated to 120 °C with monitoring of the reaction by NMR until complete consumption of the benzothiadiazole starting material (**1**). The mixture was then extracted with dichloromethane and water. The organics were dried with sodium sulfate and concentrated under reduced pressure. The crude product was purified *via* silica gel chromatography with 60% acetone/40% hexanes as the eluent to yield pure product (**(*p*-CN)$_2$DCBT**) (90 mg, 86%). ^{1}H NMR (400 MHz, $CDCl_3$) δ 8.01–7.88 (m, 8H) ppm. ^{13}C {^{1}H} NMR (100 MHz, $CDCl_3$) δ 153.8. 140.5, 136.6, 132.8, 131.2, 117.9, 115.1, 114.6, 113.4 ppm. IR (neat, cm^{-1}): 3072, 2232, 1459, 895, 876, 830, 552. HRMS ESI (negative mode) *m*/*z* calc'd for $C_{22}H_8N_6S$ $[M]^-$ 388.0531, found 388.0539.

4,7-Di-*o*-tolylbenzo[*c*][1,2,5]thiadiazole-5,6-dicarbonitrile ((tolyl)$_2$DCBT). Into a flame-dried pressure flask flushed with Ar was added benzo[*c*][1,2,5]thiadiazole-5,6-dicarbonitrile (**1**) (100 mg, 0.54 mmol), 1-bromo-2-methylbenzene (**tolyl-Br**) (202 mg, 1.18 mmol), pivalic acid (55 mg, 0.54 mmol), K_2CO_3 (223 mg, 1.61 mmol), $Pd(OAc)_2$ (6 mg, 0.027 mmol), and $[BF_4][HP(t\text{-}Bu)_2Me]$ (13 mg, 0.054 mmol) dissolved in dry toluene (1.8 mL). The flask was sealed and heated to 120 °C with monitoring of the reaction by NMR until complete consumption of the benzothiadiazole starting material (**1**). The mixture was then extracted with dichloromethane and water. The organics were dried with sodium sulfate and concentrated under reduced pressure. The crude product was purified *via* silica gel chromatography with 40% acetone/60% hexanes as the eluent to yield pure product (**(tolyl)$_2$DCBT**) (75 mg, 38%). ^{1}H NMR (400 MHz, $CDCl_3$) δ 7.56–7.34 (m, 8H), 2.23–2.17 (m, 6H) ppm. ^{13}C {^{1}H} NMR (100 MHz, $CDCl_3$) δ 154.3, 154.2, 143.0, 143.0, 136.6, 136.5, 132.6, 131.2, 131.1, 130.8, 129.8, 129.8, 126.5, 126.5, 114.7, 113.9, 20.3, 20.3 ppm. Multiple peaks present due to 2 isomers (rotamers) being present. IR (neat, cm^{-1}): 2920, 2232, 1458, 894, 758, 723, 642, 550, 447. HRMS ESI (positive mode) *m*/*z* calc'd for $C_{22}H_{15}N_4S$ $[M + H]^+$ 367.1017, found 367.1041.

Results and discussion

As previously shown, the strongly electron withdrawing nature of the DCBT core characterizes what are typically electron deficient substituents as electron donating in comparison to the core.[29] In studying this new series of dyes, computational analysis with density functional theory (DFT) was undertaken in order to better understand these electronic comparisons.

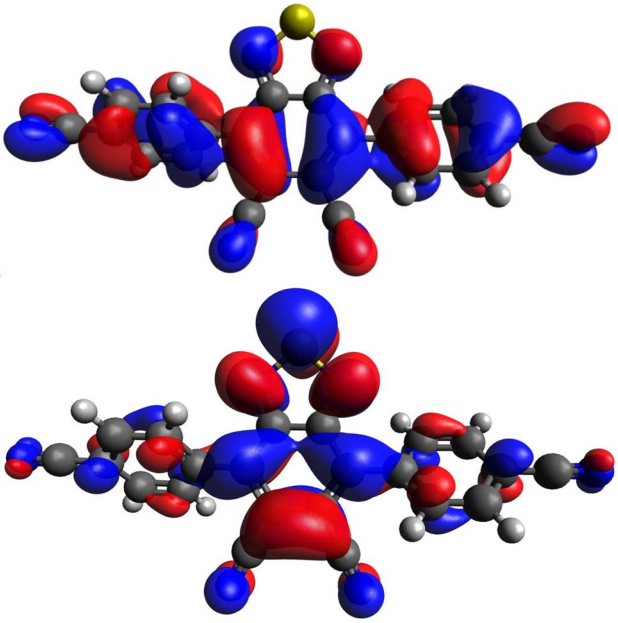

Fig. 2 Computationally derived HOMO (top) and LUMO (bottom) orbitals of (*p*-CN)$_2$DCBT using the M06-2X functional and 6-311G(d,p) basis set. Iso values are set to 0.02. Orbital images for the remaining dyes are in the ESI (Fig. S1–S7, ESI†).

Geometry optimizations were performed at the M06-2X/6-311G(d,p) level of theory[36,37] with the Gaussian 16 software package.[35] For the entire series of dyes, the highest occupied molecular orbital (HOMO) is delocalized across the entire dye, spanning from the aryl substituents to the DCBT core (Fig. 2 and S1–S7, ESI†). Likewise, the lowest unoccupied molecular orbital (LUMO) is observed to be positioned primarily on the DCBT core. Modest LUMO presence is observed on any other portion of the dyes across the entire series. This suggests that all of the aryl substituents are serving as electron donating groups in comparison to the DCBT core. The entire dye series exhibits intramolecular charge transfer (ICT) behavior, specifically as a donor–acceptor–donor system (D–A–D), for the HOMO to LUMO transition that changes regions of the molecules the orbitals are located on.

Time-dependent (TD)-DFT calculations were carried out at the M06-2X/6-311G(d,p) level of theory to better understand the orbital transitions within the series (Table 1). Calculations showed that the S_0 to S_1 transition is largely made up of the HOMO to LUMO transition in all cases (Tables 1 and S1, ESI†). The oscillator strengths for these transitions ranged from 0.2 to 0.7 which is to be expected from ICT systems. Solvatochromatic effects were studied by comparing the absorption spectra of (*p*-OHx)$_2$DCBT in solvents of varying polarity to yield a trend of red-shifting absorption as the polarity of the solvent decreased (Fig. S19†). This solvent polarity dependence further suggests the ICT behavior of this series. In comparing the HOMO and LUMO energies, it is seen that the HOMO and LUMO energies range over 2.5 eVs and 1.1 eVs respectively, suggesting that the appended groups have a greater effect on the HOMO than the LUMO.

Table 1 Computationally derived HOMO and LUMO energies, vertical transitions, and oscillator strengths from DFT at the M06-2X/6-311G(d,p) level of theory. Dyes are coded by their aryl substituents

Dyes	HOMO (eV)	LUMO (eV)	Orbitals	% Cont.	Vertical transition (nm | eV)	Oscillator strength
p-CN	−8.65	−3.23	H → L	96%	347 | 3.57	0.4667
TMS-thio	−7.41	−2.68	H → L	98%	421 | 2.95	0.5452
TAA-OHx	−6.13	−2.29	H → L	91%	495 | 2.51	0.7089
			H-2 → L	6%		
Ar-Ar-ester	−7.79	−2.75	H → L	90%	374 | 3.32	0.7356
			H-2 → L	2%		
			H-4 → L	4%		
Tolyl	−8.15	−2.60	H → L	97%	343 | 3.61	0.2192
DMA	−6.50	−2.18	H → L	96%	456 | 2.72	0.5018
TAA-(*m*-CF_3)$_4$	−7.58	−3.04	H → L	87%	406 | 3.05	0.7081
			H-2 → L	8%		
p-OHx	−7.38	−2.47	H → L	97%	394 | 3.15	0.3991

Having observed intriguing tunable energetics computationally, syntheses of the target dyes was attempted. The DCBT dyes can be accessed through a single symmetric C–H activation cross-coupling using the DCBT core (intermediate **1**)[30] and the respective aryl bromide group for each chromophore to yield the final dyes in 17–90% yield (Scheme 1). Through the entire series, one of two C–H activation conditions were used to achieve the end product.[29]

Steady-state absorption and emission spectroscopy were used to study the optical properties of the dyes (Fig. 3, Table 2). The absorption maximum spectral range spans from 363 to 567 nm in the order of tolyl = *p*-CN < Ar-Ar-Ester < *p*-OHx < TAA-(*m*-CF_3)$_4$ < TMS-thio < DMA < TAA-OHx in dichloromethane. Interestingly, (tolyl)$_2$DCBT and (*p*-CN)$_2$DCBT have the same absorption maxima despite having greatly different electronic properties in their aryl substituents which suggests sterics can have a significant influence on the energy of the charge transfer event. Despite the sterics of the tolyl group, a longer wavelength λ_{max}^{abs} is observed as part of a broad peak at 363 nm indicative of a ICT S_0 to S_1 transition for (tolyl)$_2$DCBT in comparison to the DCBT core which has sharper transitions from ~325 to 350 nm (Fig. S18†). (Ar$_2$Ester)$_2$DCBT and (*p*-OHx)$_2$DCBT follow with the third and fourth highest energy λ_{max}^{abs} values, respectively. (Ar$_2$-Ester)$_2$DCBT absorbs at a lower wavelength in comparison to (*p*-OHx)$_2$DCBT despite its extended conjugation with the extra phenyl group due to the strong electron withdrawing nature of the ester groups. Next in the series, (TAA-(*m*-CF_3)$_4$)$_2$DCBT and (TMS-thio)$_2$DCBT have very similar λ_{max}^{abs} values at 456 and 466 nm, respectively, suggesting that a withdrawn amine donor has similar electronic effects to thiophene. Finally, the two electron-rich amines, (DMA)$_2$DCBT and (TAA-OHx)$_2$DCBT exhibit absorption at the longest wavelengths of the series at

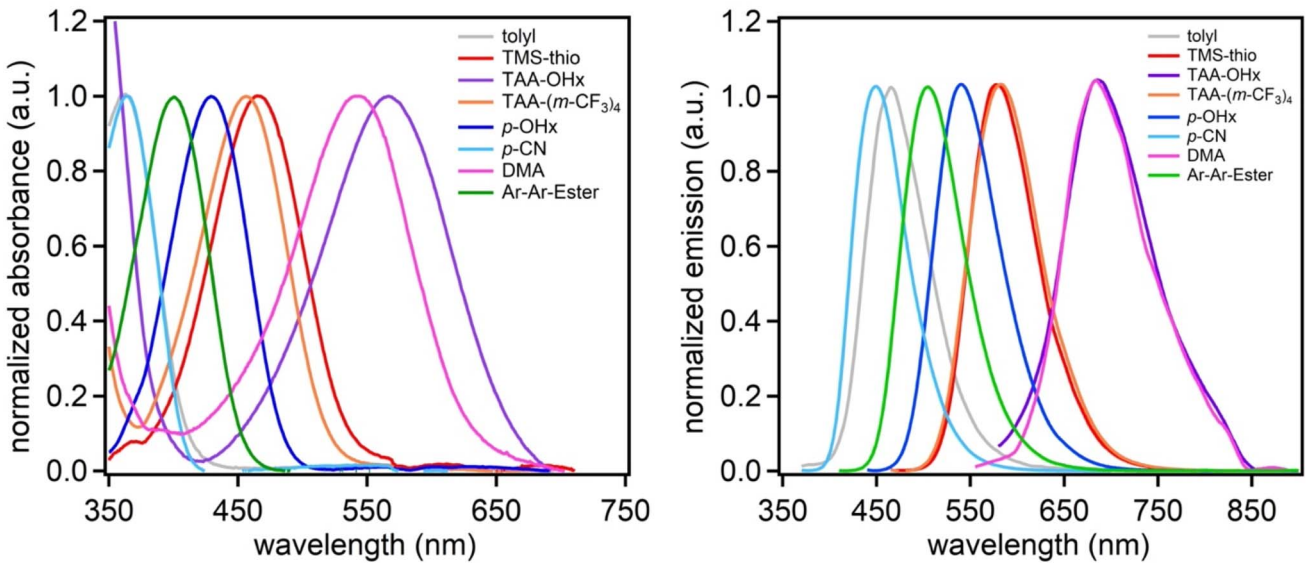

Fig. 3 Normalized absorption and emission curves in dichloromethane under argon. All absorption spectra were taken at 1×10^{-5} M except for (tolyl)$_2$DCBT which was taken at 1×10^{-4} M due to low signal. All emission spectra were taken at 1×10^{-5} M except (TAA-OHx)$_2$DCBT which was taken at 1×10^{-4} M due to low signal. Dyes are coded by their aryl substituents.

Table 2 Photophysical, electrochemical, and excited state lifetimes of the dyes in dichloromethane. Dyes are coded by their aryl substituents. * indicates a biexponential fit was used

Dye	λ_{max}^{abs} (nm)	ε (M^{-1} cm^{-1})	λ_{max}^{emis}[a] (nm)	$E_{(0-0)}$[b] (nm)	$E_{(S/S-)}$[c] (V)	$E_{(S^*/S-)}$[d] (V)	τ_{emis}[e] (ns)
p-CN	363	11 400	451	405	−0.41	2.65	2.9
TMS-thio	466	7700	581	527	−0.51	1.84	9.2
TAA-OHx	567	12 300	690	633	−0.70	1.26	6.3*
Ar-Ar-ester	401	13 600	509	452	−0.56	2.18	4.8
Tolyl	363	3200	468	412	−0.63	2.38	3.9*
DMA	542	10 600	685	623	−0.74	1.25	1.9
TAA-(*m*-CF_3)$_4$	456	12 000	583	519	−0.55	1.84	7.7
p-OHx	429	9100	543	484	−0.65	1.91	9.2
DCBT	332	13 000	370	340	−0.61	2.74	—

[a] When excited at λ_{max}^{abs}. [b] Found *via* the intercept from the normalized absorption and emission curves (Fig. S8–S16). [c] Found *via* cyclic voltammetry using a glassy carbon working electrode, platinum counter electrode, silver wire pseudo-reference electrode, 0.1 M tetrabutylammonium hexafluorophosphate as electrolyte in dichloromethane, and ferrocene as an internal standard. Value reported *versus* NHE by addition of +0.7 V *versus* ferrocene.[33,34] [d] Found *via* the equation $E_{(S^*/S-)} = E_{(S/S-)} + E_{(0-0)}$; where $E_{(0-0)}$ is converted from nm to eV by the equation eV = 1240/nm. [e] Obtained *via* fluorescence lifetime measurements in DCM (5×10^{-4} M).

542 and 567 nm, respectively. The emission maxima of the dyes follow a similar trend to the absorption maxima with minor differences. While (tolyl)$_2$DCBT and (*p*-CN)$_2$DCBT shared the same absorption maxima, (tolyl)$_2$DCBT emits at a longer wavelength than (*p*-CN)$_2$DCBT. This is likely due to the sterics of the tolyl substituent that increases reorganization energy, resulting in a larger Stokes shift. (TMS-thio)$_2$DCBT and (TAA-(*m*-CF_3)$_4$)$_2$-DCBT are observed to emit at essentially the same wavelength. Likewise, the same is seen with (DMA)$_2$DCBT and (TAA-OHx)$_2$-DCBT. The absorption and emission curve intercept ($E_{(0-0)}$) values for the series ranges from 405 to 633 nm (Fig. S8–S16, ESI†) which follows the same trend as λ_{max}^{abs} with the exception of (*p*-CN)$_2$DCBT absorbing at a lower wavelength than (tolyl)$_2$-DCBT. Additionally, the dyes exhibit molar absorptivities ranging from 3200 to 13 600 M^{-1} cm^{-1} (Table 2; Fig. S17, ESI†).

Electrochemical data was collected through cyclic voltammetry (CV) to obtain ground state reduction potentials ($E_{(S/S-)}$) of the dyes (Fig. 4). The dyes begin with neutral charge at 0.0 V *versus* NHE and are eventually reduced by 1 electron to give the dye radical anion as the CV sweep travels in the negative direction. After reduction, the potential sweep direction is switched and an electron is then removed from the radical anion dye species to give a reversible redox process. The reduction values range from −0.41 to −0.74 V *versus* normal hydrogen electrode (NHE). These values are then used to calculate the excited state reduction potential ($E_{(S^*/S-)}$) using the equation $E_{(S^*/S-)} = E_{(S/S-)} + E_{(0-0)}$ (Fig. 5). The excited state reduction potentials ranged over 1.4 V, from 1.25 to 2.65 V *vs.* NHE. However, the ground state reductions range over ∼0.3 V. This affirms the tunability of the $E_{(S^*/S-)}$ through the selection of the aryl substituents on the DCBT core and shows the wide range of photooxidants that can be generated with this molecular series. While (DMA)$_2$DCBT and (TAA-OHx)$_2$DCBT exhibit the weakest photooxidizing strengths of the series, both dyes absorb at much lower energies (greater than 540 nm) in comparison to the rest of the series which could aid in the selectivity of various chemical transformations with the use of lower energy light.

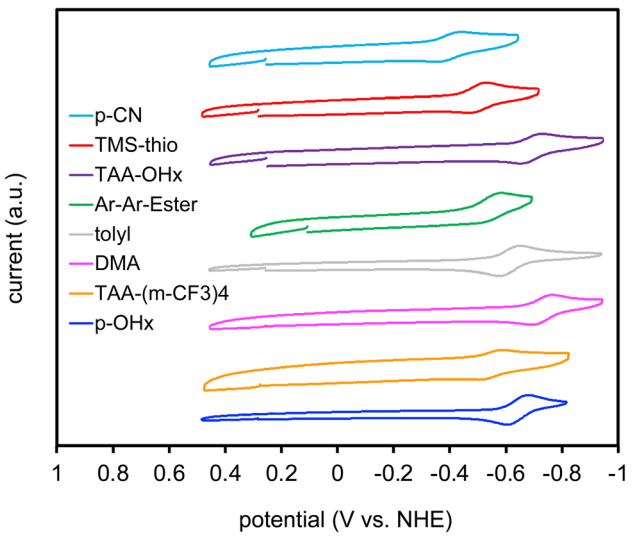

Fig. 4 Cyclic voltammograms of the DCBT dyes. Dyes are coded by their aryl substituents.

The obtained $E_{(S^*/S-)}$ value range shows that this class of DCBT photosensitizer is capable of being tuned to match or exceed the oxidizing abilities of other recent strong organic photooxidants such as the phenanthrenequinone derivatives that exhibited excited state reduction potentials ranging from 1.40 V to 1.73 V *versus* saturated calomel electrode (SCE) (or 1.64 V and 1.97 V *versus* NHE).[39] The popular acridinium dye class has been widely studied in the literature due to the strong oxidizing potentials ranging from 2.56 V to 3.05 V *versus* SCE (2.80 V to 3.29 V *versus* NHE) for the most powerful "super oxidants".[40] While the oxidizing potentials of the acridinium class surpass that presented in this work, the DCBT motif shows a large range of tunability (1.51 eV range) which can be matched to a very wide range of substrate potentials for chemical transformations.

Time-correlated single photon counting (TCSPC) was undertaken to obtain excited state lifetimes of the series. Lifetimes ranged from 1.9 to 9.2 ns (Table 2). (*p*-OHx)$_2$DCBT and

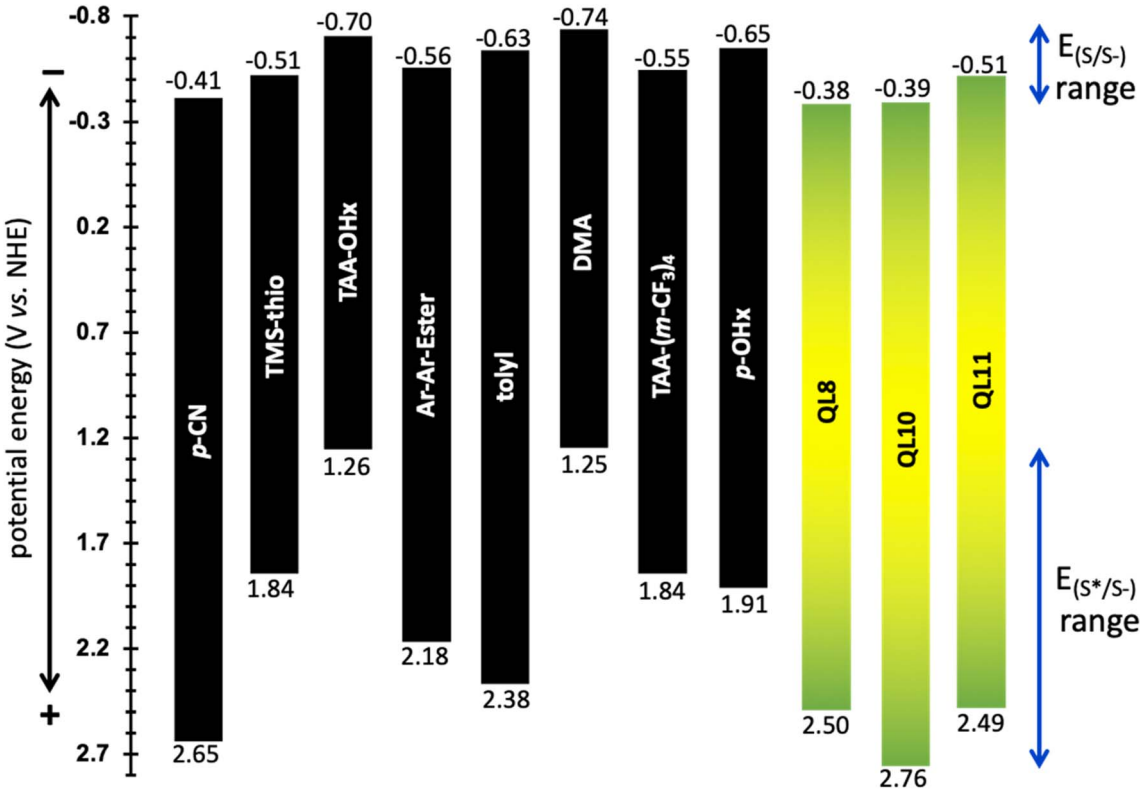

Fig. 5 Energy level diagram of the DCBT and QL dyes with $E_{(S/S-)}$ values as the top values and $E_{(S^*/S-)}$ as the bottom values. Dyes are coded by their aryl substituents.

$(TMS\text{-}thio)_2DCBT$ are observed to have the longest fluorescence lifetimes of the series. Interestingly, a general trend of increasing fluorescence lifetimes as absorption maxima increases is observed for the majority of the dyes in the series (Fig. 6). This observation goes against typical trends according to the energy gap law.[41–43] It is also important to note that $(DMA)_2DCBT$ and $(TAA\text{-}OHx)_2DCBT$ differs from the rest of the series and do not follow this trend. The reason for the deviation from the observed trend for these two derivatives is not apparent, but these two dyes both employ the strongest aryl donor groups with the least positive $E_{(S^*/S-)}$ values by more than 0.5 V. Despite $(DMA)_2DCBT$ and $(TAA\text{-}OHx)_2DCBT$ having the least positive $E_{(S^*/S-)}$ values, it is important to note that these two photooxidants are still stronger than some commonly known chemical oxidants such as "Magic Blue" and I_2. Furthermore, the oxidizing strength of these two dyes are mediated by low

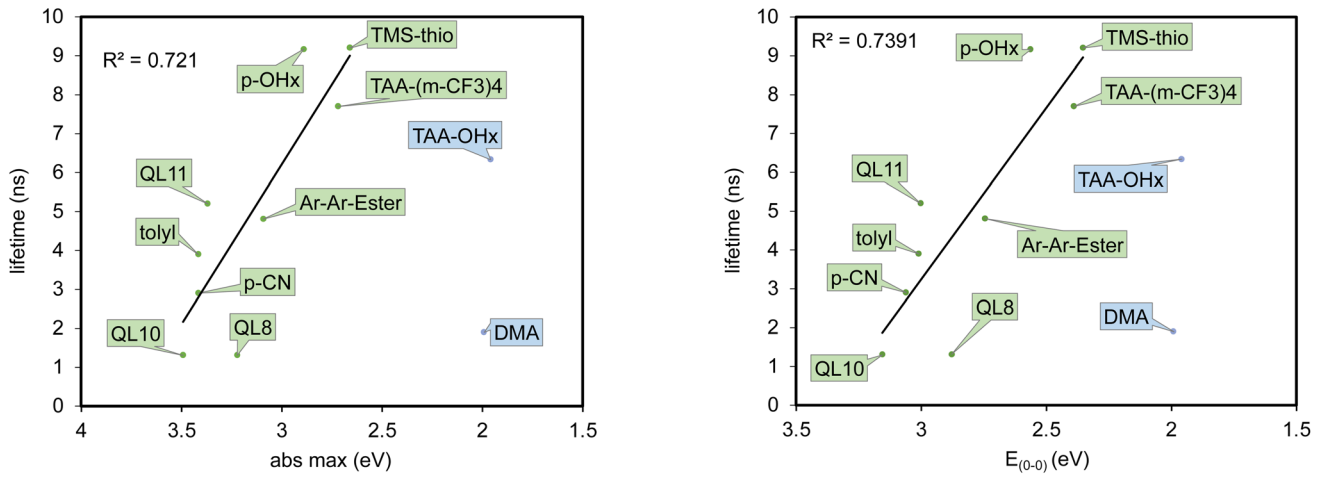

Fig. 6 Fluorescence lifetimes of DCBT dyes plotted with respect to λ_{max}^{abs} (left) and $E_{(0-0)}$ (right). Trend line and R^2 value only applies to the green dataset. Dyes are coded by their aryl substituents.

energy light (>540 nm absorption maxima; >600 nm absorption onset) which differs in comparison to other literature known photooxidants with much higher photoexcitation energy requirements (≤∼450 nm).[44] Thus, these materials may be able to drive reactions requiring strong oxidants without the use of higher energy light which is incompatible with some functionalities. As a preliminary demonstration of the thermodynamic and kinetic competence of these dyes to drive photochemical transformations, three reactions based on *p*-methoxystyrene derived substrates were undertaken showing up to 95% consumption of the starting material using 450 nm light and (*p*-OHx)$_2$DCBT to give products known in the literature (up to 29% yield with 5 turnovers) with several additional species (30–40%) (Fig. S21†).[23,45]

Conclusions

A series of DCBT dyes were synthesized and characterized computationally, electrochemically, and photophysically. Computations reveal this series to be intramolecular charge transfer systems, more specifically D–A–D systems. Electrochemical measurements showed $E_{(S^*/S-)}$ values ranging from 1.25 to 2.76 V, revealing an excited state reduction driving force range of 1.5 eV. This shows incredible energetic tunability for this class of molecules, enabling the tuning of the photooxidant to a substrate for more selective, milder reactions in some cases. Steady state absorption and emission spectroscopy was undertaken to characterize this series of dyes as visible light absorbers and emitters. Namely, (TAA-OHx)$_2$DCBT and (DMA)$_2$DCBT are lower energy visible light absorbers which allows for reaction selectivity when used in catalysis. Beyond selectivity, stronger photooxidants are necessary in order to access new chemical transformations. This was recently demonstrated with a water soluble version of QL11 named QL11-OEG; which is QL11 with oligomeric ethylene glycol chains.[28] The strong organic photooxidant QL11-OEG was shown to drive a water oxidation system which typically employs metal oxidants. The dyes put forward in this study have the potential to drive new reaction systems with tunable properties to the reaction system needs. Finally, an unexpected relationship is discovered between the excited state fluorescence lifetime and absorption maxima. This series of symmetric DCBT dyes shows the tunability of this class of photosensitizers (over a 1.5 eV range of excited state reduction potentials) as well as the suitability of these dyes for various catalytic oxidative processes. Future directions for this work include further expanding upon the energetic range of these dyes as well as further understanding and probing their excited state lifetimes *via* transient absorption spectroscopy.

Conflicts of interest

There are no conflicts to declare.

Acknowledgements

Q. Y. L., R. K., and J. H. D. thank the U.S. Department of Energy, Office of Science, Office of Basic Energy Sciences for supporting this work under award DE-SC0019131. E. C. L. and N. I. H. thank the National Science Foundation (NSF) for supporting this research with award NSF OIA-1757220 and CHE-1954922.

References

1 K. Ohkubo, K. Suga and S. Fukuzumi, Solvent-Free Selective Photocatalytic Oxidation of Benzyl Alcohol to Benzaldehyde by Molecular Oxygen Using 9-Phenyl-10-Methylacridinium, *Chem. Commun.*, 2006, **19**, 2018–2020.
2 M. Uygur, J. H. Kuhlmann, M. C. Pérez-Aguilar, D. G. Piekarski and O. García Mancheño, Metal- and Additive-Free C–H Oxygenation of Alkylarenes by Visible-Light Photoredox Catalysis, *Green Chem.*, 2021, **23**, 3392–3399.
3 D. Steuernagel and H.-A. Wagenknecht, Photocatalytic Synthesis of Acetals and Ketals from Aldehydes and Silylenolethers without the Use of Acids, *Chem.–Eur. J.*, 2023, **29**, e202203767.
4 P. P. Singh, J. Singh and V. Srivastava, Visible-Light Acridinium-Based Organophotoredox Catalysis in Late-Stage Synthetic Applications, *RSC Adv.*, 2023, **13**, 10958–10986.
5 Z. Luo, C. Lu, G. Histand and D. Lin, One-Step Visible Light Photoredox-Catalyzed Purine C8 Alkoxylation with Alcohol, *J. Org. Chem.*, 2022, **87**, 11558–11564.
6 X. Kan, J.-C. Wang, Z. Chen, J.-Q. Du, J.-L. Kan, W.-Y. Li and Y.-B. Dong, Synthesis of Metal-Free Chiral Covalent Organic Framework for Visible-Light-Mediated Enantioselective Photooxidation in Water, *J. Am. Chem. Soc.*, 2022, **144**, 6681–6686.
7 E. Skolia, P. L. Gkizis, N. F. Nikitas and C. G. Kokotos, Photochemical Aerobic Oxidation of Sulfides to Sulfoxides: The Crucial Role of Wavelength Irradiation, *Green Chem.*, 2022, **24**, 4108–4118.
8 B. Zilate, C. Fischer and C. Sparr, Design and Application of Aminoacridinium Organophotoredox Catalysts, *Chem. Commun.*, 2020, **56**, 1767–1775.
9 A. Y. Chan, I. B. Perry, N. B. Bissonnette, B. F. Buksh, G. A. Edwards, L. I. Frye, O. L. Garry, M. N. Lavagnino, B. X. Li, Y. Liang, E. Mao, A. Millet, J. V. Oakley, N. L. Reed, H. A. Sakai, C. P. Seath and D. W. C. MacMillan, Metallaphotoredox: The Merger of Photoredox and Transition Metal Catalysis, *Chem. Rev.*, 2022, **122**, 1485–1542.
10 A. B. Muñoz-García, I. Benesperi, G. Boschloo, J. J. Concepcion, J. H. Delcamp, E. A. Gibson, G. J. Meyer, M. Pavone, H. Pettersson, A. Hagfeldt and M. Freitag, Dye-Sensitized Solar Cells Strike Back, *Chem. Soc. Rev.*, 2021, **50**, 12450–12550.
11 D. Zhang, M. Stojanovic, Y. Ren, Y. Cao, F. T. Eickemeyer, E. Socie, N. Vlachopoulos, J.-E. Moser, S. M. Zakeeruddin, A. Hagfeldt and M. Grätzel, A Molecular Photosensitizer Achieves a Voc of 1.24 V Enabling Highly Efficient and Stable Dye-Sensitized Solar Cells with Copper(II/I)-Based Electrolyte, *Nat. Commun.*, 2021, **12**, 1777.

12 Y. H. Hong, Y.-M. Lee, W. Nam and S. Fukuzumi, Molecular Photocatalytic Water Splitting by Mimicking Photosystems I and II, *J. Am. Chem. Soc.*, 2022, **144**, 695–700.
13 D. Antón-García, J. Warnan and E. Reisner, A Diketopyrrolopyrrole Dye-Based Dyad on a Porous TiO2 Photoanode for Solar-Driven Water Oxidation, *Chem. Sci.*, 2020, **11**, 12769–12776.
14 X. M. C. Ta, R. Daiyan, T. K. A. Nguyen, R. Amal, T. Tran-Phu and A. Tricoli, Alternatives to Water Photooxidation for Photoelectrochemical Solar Energy Conversion and Green H_2 Production, *Adv. Energy Mater.*, 2022, **12**, 2201358.
15 Q. Li, Y. Ouyang, H. Li, L. Wang and J. Zeng, Photocatalytic Conversion of Methane: Recent Advancements and Prospects, *Angew. Chem., Int. Ed.*, 2022, **61**, e202108069.
16 M. D. Kärkäs, E. V. Johnston, O. Verho and B. Åkermark, Artificial Photosynthesis: From Nanosecond Electron Transfer to Catalytic Water Oxidation, *Acc. Chem. Res.*, 2014, **47**, 100–111.
17 R. R. Rodrigues, A. Peddapuram, A. L. Dorris, N. I. Hammer and J. H. Delcamp, Thienopyrroledione-Based Photosensitizers as Strong Photoinduced Oxidants: Oxidation of $Fe(Bpy)_3^{2+}$ in a >1.3 V Dye-Sensitized Solar Cell, *ACS Appl. Energy Mater.*, 2019, **2**, 5547–5556.
18 R. R. Rodrigues, H. Cheema and J. H. Delcamp, A High-Voltage Molecular-Engineered Organic Sensitizer–Iron Redox Shuttle Pair: 1.4 V DSSC and 3.3 V SSM-DSSC Devices, *Angew. Chem., Int. Ed.*, 2018, **57**, 5472–5476.
19 Y. Lee and M. S. Kwon, Emerging Organic Photoredox Catalysts for Organic Transformations, *Eur. J. Org Chem.*, 2020, **2020**, 6028–6043.
20 J. Moon, Y. K. Moon, D. D. Park, S. Choi, Y. You and E. J. Cho, Visible-Light-Induced Trifluoromethylation of Unactivated Alkenes with Tri(9-Anthryl)Borane as an Organophotocatalyst, *J. Org. Chem.*, 2019, **84**, 12925–12932.
21 T. Bortolato, S. Cuadros, G. Simionato and L. Dell'Amico, The Advent and Development of Organophotoredox Catalysis, *Chem. Commun.*, 2022, **58**, 1263–1283.
22 A. Tlili and S. Lakhdar, Acridinium Salts and Cyanoarenes as Powerful Photocatalysts: Opportunities in Organic Synthesis, *Angew. Chem.*, 2021, **133**, 19678–19701.
23 N. A. Romero and D. A. Nicewicz, Mechanistic Insight into the Photoredox Catalysis of Anti-Markovnikov Alkene Hydrofunctionalization Reactions, *J. Am. Chem. Soc.*, 2014, **136**, 17024–17035.
24 G. Han, G. Li, J. Huang, C. Han, C. Turro and Y. Sun, Two-Photon-Absorbing Ruthenium Complexes Enable near Infrared Light-Driven Photocatalysis, *Nat. Commun.*, 2022, **13**, 2288.
25 L. Mei, J. M. Veleta and T. L. Gianetti, Helical Carbenium Ion: A Versatile Organic Photoredox Catalyst for Red-Light-Mediated Reactions, *J. Am. Chem. Soc.*, 2020, **142**, 12056–12061.
26 R. Obertík, J. Chudoba, J. Šturala, J. Tarábek, L. Ludvíková, T. Slanina, B. König and R. Cibulka, Highly Chemoselective Catalytic Photooxidations by Using Solvent as a Sacrificial Electron Acceptor, *Chem.–Eur. J.*, 2022, **28**, e202202487.
27 S. P. Pitre, C. D. McTiernan, W. Vine, R. DiPucchio, M. Grenier and J. C. Scaiano, Visible-Light Actinometry and Intermittent Illumination as Convenient Tools to Study $Ru(Bpy)_3Cl_2$ Mediated Photoredox Transformations, *Sci. Rep.*, 2015, **5**, 16397.
28 Q. Y. Li, L. A. Hunt, K. H. Wijesinghe, C. Curiac, A. Williams, A. Dass, N. I. Hammer and J. H. Delcamp, Dicyanobenzothiadiazole (DCBT) Organic Dye as a Visible Light Absorbing Strong Photoinduced Oxidant with a 16 Microsecond Long-Lived Excited State, *Adv. Energy Mater.*, 2023, **13**, 2203102.
29 J. Zhang, T. C. Parker, W. Chen, L. Williams, V. N. Khrustalev, E. V. Jucov, S. Barlow, T. V. Timofeeva and S. R. Marder, C–H-Activated Direct Arylation of Strong Benzothiadiazole and Quinoxaline-Based Electron Acceptors, *J. Org. Chem.*, 2016, **81**, 360–370.
30 C. Burmester and R. Faust, A Reliable Route to 1,2-Diamino-4,5-Phthalodinitrile, *Synthesis*, 2008, 1179–1181.
31 J. H. Delcamp, A. Yella, M. K. Nazeeruddin and M. Grätzel, Modulating dye $E_{(S+/S*)}$ with Efficient Heterocyclic Nitrogen Containing Acceptors for DSCs, *Chem. Commun.*, 2012, **48**, 2295–2297.
32 E. Zhu, J. Hai, Z. Wang, B. Ni, Y. Jiang, L. Bian, F. Zhang and W. Tang, Two-Dimensional Polyfluorenes Bearing Thienylenevinylene π-Bridge-Acceptor Side Chains for Photovoltaic Solar Cells, *J. Phys. Chem. C*, 2013, **117**, 24700–24709.
33 N. G. Connelly and W. E. Geiger, Chemical Redox Agents for Organometallic Chemistry, *Chem. Rev.*, 1996, **96**, 877–910.
34 R. C. Weast and M. J. Astle, *CRC Handbook of Chemistry and Physics: A Ready-Reference Book of Chemical and Physical Data*, The CRC Press, Boca Raton, Fla., 63rd edn, 1982, pp. 1982–1983.
35 M. J. Frisch, G. W. Trucks, H. B. Schlegel, G. E. Scuseria, M. A. Robb, J. R. Cheeseman, G. Scalmani, V. Barone, G. A. Petersson, H. Nakatsuji, X. Li, M. Caricato, A. V. Marenich, J. Bloino, B. G. Janesko, R. Gomperts, B. Mennucci, H. P. Hratchian, J. V. Ortiz, A. F. Izmaylov, J. L. Sonnenberg, D. Williams-Young, F. Ding, F. Lipparini, F. Egidi, J. Goings, B. Peng, A. Petrone, T. Henderson, D. Ranasinghe, V. G. Zakrzewski, J. Gao, N. Rega, G. Zheng, W. Liang, M. Hada, M. Ehara, K. Toyota, R. Fukuda, J. Hasegawa, M. Ishida, T. Nakajima, Y. Honda, O. Kitao, H. Nakai, T. Vreven, K. Throssell, J. A. Montgomery Jr., J. E. Peralta, F. Ogliaro, M. J. Bearpark, J. J. Heyd, E. N. Brothers, K. N. Kudin, V. N. Staroverov, T. A. Keith, R. Kobayashi, J. Normand, K. Raghavachari, A. P. Rendell, J. C. Burant, S. S. Iyengar, J. Tomasi, M. Cossi, J. M. Millam, M. Klene, C. Adamo, R. Cammi, J. W. Ochterski, R. L. Martin, K. Morokuma, O. Farkas, J. B. Foresman and D. J. Fox, *Gaussian 16, Revision C.01*, Gaussian, Inc., Wallingford CT, 2016.
36 Y. Zhao and D. G. Truhlar, The M06 Suite of Density Functionals for Main Group Thermochemistry, Thermochemical Kinetics, Noncovalent Interactions, Excited States, and Transition Elements: Two New Functionals and Systematic Testing of Four M06-Class

Functionals and 12 Other Functionals, *Theor. Chem. Acc.*, 2008, **120**, 215–241.

37 M. J. Frisch, J. A. Pople and J. S. Binkley, Self-consistent Molecular Orbital Methods 25. Supplementary Functions for Gaussian Basis Sets, *J. Chem. Phys.*, 1984, **80**, 3265–3269.

38 F. Mo, D. Qiu, Y. Jiang, Y. Zhang and J. Wang, A Base-Free, One-Pot Diazotization/Cross-Coupling of Anilines with Arylboronic Acids, *Tetrahedron Lett.*, 2011, **52**, 518–522.

39 J. Talvitie, I. Alanko, A. Lenarda, N. Durandin, N. Tkachenko, M. Nieger and J. Helaja, Electron-Deficient Phenanthrenequinone Derivative for Photoactivated Hydrogen Atom Transfer Mediated Oxidation of Secondary Alcohols, *ChemPhotoChem*, 2023, **7**, e202300107.

40 J. Žurauskas, S. Boháčová, S. Wu, V. Butera, S. Schmid, M. Domański, T. Slanina and J. P. Barham, Electron-Poor Acridones and Acridiniums as Super Photooxidants in Molecular Photoelectrochemistry by Unusual Mechanisms, *Angew. Chem., Int. Ed.*, 2023, **62**, e202307550.

41 S. J. A. Jang, Simple Generalization of the Energy Gap Law for Nonradiative Processes, *J. Chem. Phys.*, 2021, **155**, 164106.

42 J. V. Caspar, E. M. Kober, B. P. Sullivan and T. J. Meyer, Application of the Energy Gap Law to the Decay of Charge-Transfer Excited States, *J. Am. Chem. Soc.*, 1982, **104**, 630–632.

43 R. Englman and J. Jortner, The Energy Gap Law for Radiationless Transitions in Large Molecules, *Mol. Phys.*, 1970, **18**, 145–164.

44 C. K. Prier, D. A. Rankic and D. W. C. MacMillan, Visible Light Photoredox Catalysis with Transition Metal Complexes: Applications in Organic Synthesis, *Chem. Rev.*, 2013, **113**, 5322–5363.

45 D. S. Hamilton and D. A. Nicewicz, Direct Catalytic Anti-Markovnikov Hydroetherification of Alkenols, *J. Am. Chem. Soc.*, 2012, **134**, 18577–18580.